Available online at www.sciencedirect.com

SCIENCE DIRECT®

Lithos 86 (2006) 245–259

LITHOS

www.elsevier.com/locate/lithos

Water content in natural eclogite and implication for water transport into the deep upper mantle

Ikuo Katayama *, Satoru Nakashima [1], Hisayoshi Yurimoto [2]

Department of Earth and Planetary Sciences, Tokyo Institute of Technology, Tokyo 152-8551, Japan

Received 8 March 2005; accepted 27 June 2005
Available online 15 August 2005

Abstract

Infrared spectroscopy and ion micro-probe measurements showed that the major constituent minerals of eclogites from the Kokchetav massif, which have been subducted to ~180 km depths, contain significant amounts of water up to 870 ppm H_2O (by weight) in omphacite, 130 ppm H_2O in garnet and 740 ppm H_2O in rutile. Omphacite shows three hydroxyl absorption bands at 3440–3460, 3500–3530 and 3600–3625 cm^{-1}, garnet has a single band at 3580–3630 cm^{-1} and rutile has a single sharp band at 3280 cm^{-1}. The hydroxyl absorbance at these wavenumbers changes with the crystal orientation in polarized infrared radiation, indicating that the water is structurally incorporated in these minerals. The water contents in omphacite and garnet increase systematically with the metamorphic pressure of the host eclogites. The partitioning coefficient of the water content between coexisting garnet and omphacite is similar in different eclogites, $D^{Grt/Omp}$~0.1–0.2, but decreases slightly at high pressure. Based on the mineral proportions of the eclogites, we estimate bulk-rock water content in the eclogites ranging from 3070 to 300 ppm H_2O (by weight). Although hydrous minerals are absent in the diamond-grade eclogite (~60 kbar and ~1000 °C), trace amounts of water are incorporated in the nominally anhydrous minerals such as omphacite and garnet. The presence of significant water in these minerals implies that the subducting oceanic crust can transport considerable amounts of water into the deep upper mantle beyond the stability of hydrous minerals. Such water may be stored in the deep upper mantle and have an important influence on dynamics in the Earth's interior.

Keywords: Water; Eclogite; Ultrahigh-pressure metamorphism; Subducting crust

1. Introduction

Water is largely introduced into basaltic crust by hydrothermal alternation at mid-oceanic ridge (e.g., Staudigel et al., 1995), and is recycled into the mantle by subduction of oceanic lithosphere. The presence of water plays an important role in the melting behavior and the physical properties of minerals and rocks

* Corresponding author. Present address: Department of Geology and Geophysics, Yale University, CT 06520, USA. Tel.: +1 203 432 5990; fax: +1 203 432 3134.
E-mail address: ikuo.katayama@yale.edu (I. Katayama).
[1] Present address: Department of Earth and Space Science, Osaka University, Osaka 560-0043, Japan.
[2] Present address: Department of Earth and Planetary Sciences, Hokkaido University, Hokkaido 060-0810, Japan.

0024-4937/$ - see front matter © 2005 Elsevier B.V. All rights reserved.
doi:10.1016/j.lithos.2005.06.006

(e.g., Thompson, 1992; Iwamori, 1998; Karato, 2003). Therefore, understanding the distribution of water is key for island arc magmatism and earthquakes at convergent plate boundaries, as well as mantle dynamics in the Earth's interior. To evaluate the distribution of water in subducted lithosphere, phase relations in H_2O-bearing basaltic composition have been systematically investigated by high-pressure and high-temperature experiments (e.g., Poli and Schmidt, 1995; Schmidt and Poli, 1998; Ono, 1998; Okamoto and Maruyama, 1999). These experiments have shown that most water is released during the amphibolite–eclogite transformation at shallow depths (~50 km). Trace amounts of water can also be accommodated in lawsonite or phengite, up to depths of 300 km, in cold subduction zones. However, for a relatively normal subduction geotherm (Maruyama et al., 1996), all hydrous minerals in basaltic crust become unstable at pressures over 30 kbar and temperatures over 800 °C. For this reason, it is generally considered that the basaltic layer cannot carry significant amounts of water into the deeper mantle.

However, nominally anhydrous minerals have been found to dissolve considerable amounts of water (e.g., Bell and Rossman, 1992a). Garnet and pyroxenes from mantle-derived xenoliths contain up to 200 and 1000 ppm wt H_2O, respectively (Bell and Rossman, 1992a; Smyth et al., 1991). High-pressure experiments have also reported substantial water solubility in garnet (Ackermann et al., 1983; Geiger et al., 1991; Lu and Keppler, 1997; Withers et al., 1998) and pyroxenes (Skogby, 1994; Rauch and Keppler, 2002; Bromiley and Keppler, 2004). These observations indicate that trace amounts of water are capable of being recycled into the deep upper mantle beyond the stability of hydrous minerals in subducting oceanic crust.

In this study, we collected natural eclogites from the diamond-bearing Kokchetav ultrahigh-pressure (UHP) metamorphic terrane, which have been subducted to mantle depths around ~180 km; peak metamorphic conditions are reported to be pressures of ~60 kbar and temperatures of ~1000 °C (Okamoto et al., 2000). The eclogites are mainly composed of garnet and omphacite with minor rutile and SiO_2 phase. No hydrous minerals are recognized in the diamond-grade sample, although minor amphibole, zoisite and phengite occur in relatively low-pressure eclogites. Although a previous study has measured the water content of omphacite using infrared (IR) micro-spectroscopy (Katayama and Nakashima, 2003), here we used secondary ion mass spectrometry (SIMS) as well as IR spectroscopy to quantify the trace amounts of water in all of the major constituent minerals of the eclogites, including omphacite, garnet, rutile and coesite. Note that it is difficult to eliminate the effect of later-stage water loss or addition due to the fast diffusion rate of hydrogen in these minerals (e.g., Wang et

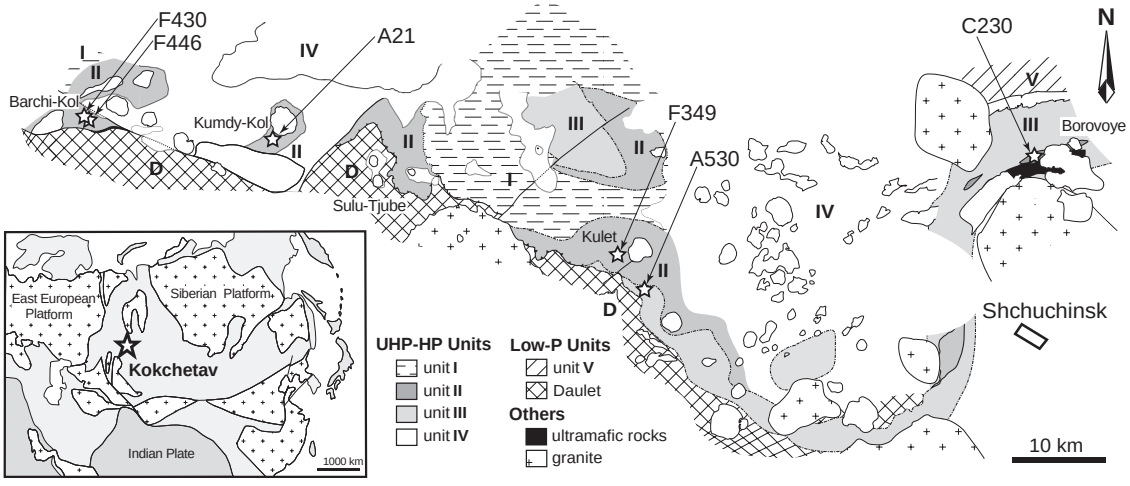

Fig. 1. Geological map of the Kokchetav UHP–HP massif modified after Kaneko et al. (2000). Sample localities are shown with corresponding sample numbers. Insert map shows the location of the Kokchetav massif in the Eurasian continent.

al., 1996; Carpenter et al., 2000). Evidences from high-grade metamorphic rocks can provide insight into the capability of water incorporation in natural systems, which may produce more realistic hydratable defects in the crystals.

2. Geological outline

The Kokchetav massif contains abundant microdiamonds in the crustal materials (Sobolev and Shatsky, 1990), which indicates the supracrustal rocks were once subducted to depths over ~120 km and then returned to the surface. Therefore, these rocks can provide important information on the dynamics of the subducted lithosphere in the deep upper mantle, which has attracted considerable attention to these unique rocks and their metamorphic evolution (e.g., Sobolev and Shatsky, 1990; Zhang et al., 1997; Okamoto et al., 2000; Ogasawara et al., 2000; Katayama et al., 2001). The massif is situated in the central domain of the composite Eurasian craton, and was formed during Cambrian collisional orogenic events (Dobretsov et al., 1995). It is composed of several Precambrian rock series, Cambro–Ordovician volcanic and sedimentary rocks, and Carboniferous–Triassic shallow-water and lacustrine sediments (Dobretsov et al., 1995). The UHP–HP metamorphic section is a thin (1–2 km), more or less coherent, subhorizontal sheet, which is structurally overlain by a weakly metamorphosed unit, and underlain by the Daulet Suite (Fig. 1; Kaneko et al., 2000).

The UHP–HP section is subdivided into four units based on their predominant lithological and metamorphic assemblages (Kaneko et al., 2000). Unit I occupies the lowest structural level and is composed of amphibolite and quartzofelspathic gneiss. Unit II is sandwiched between unit I and III, and is predominantly composed of pelitic–psammitic gneiss with locally abundant eclogite blocks. Metamorphic diamond and coesite occur in this unit. Eclogites occur as lenticular masses a meter to a few kilometers in size, which are surrounded by country gneisses or marbles. They are concentrated in several regions including, Barchi-Kol, Kumdy-Kol, Chagkinka, Sulu–Tjube, Enbek–Berlyk, Kulet, Soldat-Kol and Borovoye. Unit III structurally overlies unit II and is composed of alternating orthogneiss and amphibolite with rare eclogite lenses. Unit IV is the structural top of the UHP–HP unit and is mainly composed of siliceous schist. These UHP–HP units were intruded by post-orogenic Ordovician–Silurian granitoids (Dobretsov et al., 1995).

3. Petrography and mineral chemistry

We chose six eclogite samples from various *P–T* conditions for the water content analysis. The metamorphic conditions are shown in Fig. 2 and the

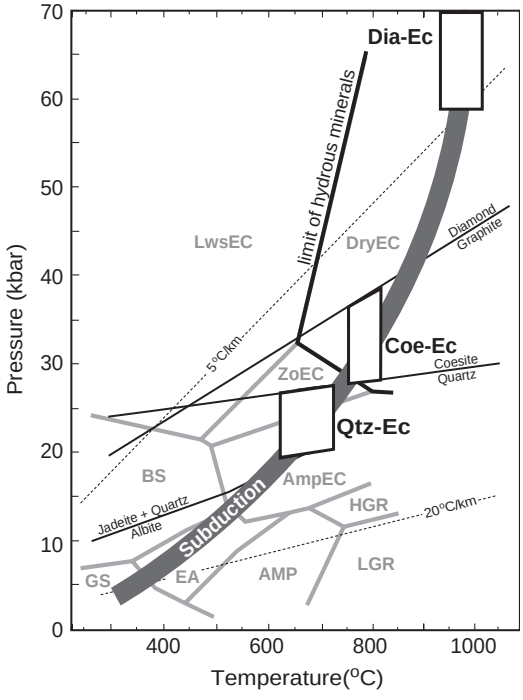

Fig. 2. Pressure–temperature conditions of analyzed eclogites from the Kokchetav UHP–HP massif, Dia–Ec: diamond–grade eclogite, Coe–Ec: coesite–eclogite, Qtz–Ec: quartz–eclogite. Geotherms of 5 and 20 °C/km are also shown for reference. Thick lines are the limits of hydrous minerals in mid-ocean ridge basalt (MORB) composition (Okamoto and Maruyama, 1999). Abbreviations, GS: greenschist facies, EA: epidote–amphibolite facies, Am: amphibolite facies, LGR: low-pressure granulite facies, HGR: high-pressure granulite facies, BS: blueschist facies, AmpEC: amphibole eclogite facies, ZoEC: zoisite eclogite facies, LwsEC: lawsonite eclogite facies, DryEC: dry eclogite facies. Petrogenic grids, subdivision of eclogite facies and wet solidus are from Schmidt and Poli (1998) and Okamoto and Maruyama (1999), and reaction curves of diamond–graphite, coesite–quartz and jadeite–quartz–albite from Bundy (1980), Bohlen and Boettcher (1982), and Holland (1980).

Table 1
Mineral parageneses and *P–T* conditions of the eclogites

Sample	Rock type	Mineral assemblage	Pressure	Temperature
A21	Dia–Ec*	Omp+Grt+Coe/Qtz+Rt	50–70 kbar	940–1020 °C
F430	Coe–Ec	Omp+Grt+Coe/Qtz+Rt	28–38 kbar	770–800 °C
F446	Coe–Ec	Omp+Grt+Coe/Qtz+Phn+Rt	34–39 kbar	770–790 °C
A530	Qtz–Ec	Omp+Grt+Amp+Qtz+Rt	20–27 kbar	610–660 °C
C230	Qtz–Ec	Omp+Grt+Amp+Qtz+Phn+Rt	24–26 kbar	690–730 °C
F349	Qtz–Ec	Omp+Grt+Amp+Qtz+Rt	20–27 kbar	660–680 °C

*Diamond is absent in the eclogite, but occurs in surrounding pelitic gneisses and marble. *P–T* conditions were estimated from polymorph mineral relations (Bundy, 1980; Bohlen and Boettcher, 1982) and geothermobarometers (Ellis and Green, 1979; Carswell et al., 1997; Okamoto et al., 2000). Mineral abbreviations; Coe: coesite, Omp: omphacite, Grt: garnet, Amp: amphibole, Qtz: quartz, Rt: rutile, Phn: phengite.

mineral assemblages of each eclogite are summarized in Table 1. A diamond-grade eclogite (Dia–Ec) consists of garnet+omphacite+rutile+coesite/quartz with minor amounts of apatite and zircon. Diamond is absent in the eclogite due to unfavorable bulk composition, but is abundant in surrounding pelitic gneisses and dolomitic marble (Sobolev and Shatsky, 1990; Katayama et al., 2000a; Ogasawara et al., 2000). Coesite occurs as tiny inclusions in zircon and omphacite. The metamorphic peak *P–T* conditions are estimated to be 50–70 kbar and 940–1020 °C based on the K_2O-in-pyroxene geobarometer (Okamoto et al., 2000) and the garnet–clinopyroxene geothermometer (Ellis and Green, 1979). Coesite–eclogites (Coe–Ec) are composed of omphacite+garnet+coesite/quartz+-rutile±phengite. The garnet and omphacite of the

Table 2
Representative compositions of omphacite and garnet in the eclogites

Rock type	Omphacite							Garnet					
sample	Dia–Ec		Coe–Ec		Qtz–Ec			Dia–Ec	Coe–Ec		Qtz–Ec		
	A21-inc08	A21-08	F430-12	F446-09	A530-08	C230-01	F349-08	A21-08	F430-06	F446-09	A530-08	C230-10	F349-09
wt.% oxides													
SiO_2	55.75	55.91	55.16	54.77	55.23	55.27	55.44	39.78	38.83	38.57	38.11	38.14	38.53
TiO_2	0.24	0.16	0.17	0.09	0.09	0.05	0.09	0.31	0.11	0.03	0.25	0.00	0.00
Al_2O_3	9.70	9.10	9.02	8.08	9.09	8.97	8.64	21.77	21.88	21.67	21.17	21.68	21.58
Cr_2O_3	0.00	0.01	0.00	0.00	0.00	0.05	0.00	0.00	0.08	0.00	0.00	0.01	0.03
FeO*	5.89	5.66	4.62	5.88	7.39	5.41	7.31	20.00	22.95	24.32	27.04	25.27	28.61
MnO	0.05	0.04	0.08	0.00	0.02	0.03	0.04	0.29	0.46	0.52	0.58	0.51	0.46
MgO	8.56	9.06	9.54	9.61	7.71	9.03	8.40	5.29	5.51	4.60	2.71	4.71	4.67
CaO	14.45	14.00	16.69	16.41	13.41	14.44	14.03	13.29	9.67	10.02	9.97	8.77	6.39
Na_2O	5.32	5.53	4.61	4.77	6.47	6.01	5.95	0.12	0.03	0.05	0.07	0.02	0.06
K_2O	0.07	0.03	0.02	0.00	0.00	0.00	0.00	0.02	0.01	0.00	0.00	0.00	0.00
Total	100.02	99.51	99.90	99.61	99.40	99.24	99.89	100.87	99.52	99.78	99.88	99.10	100.33
Cations per 6 oxygen atoms								*Cations per 12 oxygen atoms*					
Si	1.998	2.011	1.982	1.987	2.009	2.000	2.007	3.017	3.010	3.007	3.010	2.999	3.013
Ti	0.006	0.004	0.005	0.002	0.002	0.001	0.002	0.014	0.006	0.002	0.015	0.000	0.000
Al	0.410	0.386	0.382	0.346	0.390	0.382	0.368	1.937	1.999	1.991	1.971	2.009	1.989
Cr	0.000	0.000	0.000	0.000	0.000	0.001	0.000	0.000	0.005	0.000	0.000	0.001	0.002
Fe	0.177	0.170	0.139	0.178	0.225	0.164	0.221	1.346	1.488	1.586	1.786	1.662	1.871
Mn	0.001	0.001	0.002	0.000	0.001	0.001	0.001	0.028	0.030	0.034	0.039	0.034	0.030
Mg	0.458	0.486	0.511	0.520	0.418	0.487	0.453	0.614	0.637	0.534	0.319	0.552	0.545
Ca	0.555	0.540	0.642	0.638	0.522	0.560	0.544	1.039	0.804	0.837	0.844	0.739	0.535
Na	0.370	0.386	0.321	0.335	0.456	0.421	0.417	0.008	0.004	0.008	0.010	0.002	0.009
K	0.003	0.001	0.001	0.000	0.000	0.000	0.000	0.001	0.001	0.000	0.000	0.000	0.000

*Total Fe calculated as FeO.

coesite–eclogites contain pseudomorphs after coesite, which consist of polycrystalline quartz aggregates with intense radial fractures in their host minerals. Geothermobarometers yielded 28–39 kbar and 770–800 °C for metamorphic conditions of the coesite–eclogites. Quartz–eclogites (Qtz–Ec) commonly contain hydrous minerals such as amphibole, zoisite or phengite, which were formed at 20–27 kbar and 610–730 °C.

Omphacites in each eclogite are mostly homogeneous; jadeite components vary from X_{Jd} 0.32–0.40 in different samples (Table 2). Matrix omphacite in the diamond-grade eclogite contains crystallographically oriented quartz rods, which are a few μm in width and about 100 μm in length. On the other hand, zircon-hosted omphacite inclusions from the same sample do not show the quartz exsolution, and electron-microprobe analysis indicates a significant Ca–Eskola component ($Ca_{0.5}\square_{0.5}AlSi_2O_6$, where □ is a vacancy on the M_2 site) in the omphacite inclusions, up to 9.6 mol%. Because the matrix omphacite contains abundant quartz exsolution lamellae, the original composition was recalculated based on its quartz content. The resulting original omphacite contains 6.6 mol% Ca–Eskola component, which is similar to the composition of the inclusions in zircon (Katayama et al., 2000b). The primary pyroxene at the peak UHP metamorphic conditions therefore contains a high Ca–Eskola component, which indicates that there were a large number of vacancies on the M_2 site. In the other eclogites, the quartz exsolution was absent in omphacites; these have relatively low Ca–Eskola component (0.3–2.8 mol%).

Representative garnet compositions are shown in Table 2. Garnets show systematic compositional changes with metamorphic condition, in which the pyrope and grossular components increase with increasing pressure, up to 21 and 36 mol%, respectively. Garnets from the diamond–eclogite contain detectable Na_2O (up to 0.12 wt.%), whereas it is negligible in the other eclogites. Most garnets in the diamond- and coesite-grade eclogites are chemically homogeneous. In contrast, garnets from the quartz–eclogites show slight chemical zonation with an increasing pyrope component from core to rim. In these grains, we used the pyrope-rich rim parts for the water content analysis.

The eclogites commonly contains rutile as an accessory mineral. The rutiles contain trace amounts of trivalent elements such as Cr_2O_3 (~0.09 wt.%), Al_2O_3 (~0.03 wt.%) and Fe_2O_3 (~0.21 wt.%), but these trace elements have no systematic differences between each eclogite. Coesite was rarely identified as inclusions in zircon and omphacite. Most of coesite in omphacite were completely transformed to quartz aggregates with intense radial fractures in the host minerals. On the other hand, zircon preserves coesite without the back-transformation. However, the coesite inclusions in zircon are too small to analyze water content by FTIR or SIMS. We therefore prepared coarse-grained coesites preserved in garnets from the Western Alps and the Dabie–Sulu UHP terranes. The metamorphic conditions for these samples are 37 kbar and 800 °C for the Western Alps (Schertl et al., 1991), and >27 kbar and >670 °C for the Dabie–Sulu region (Omori et al., 1998). These coesites were nearly pure SiO_2 in composition.

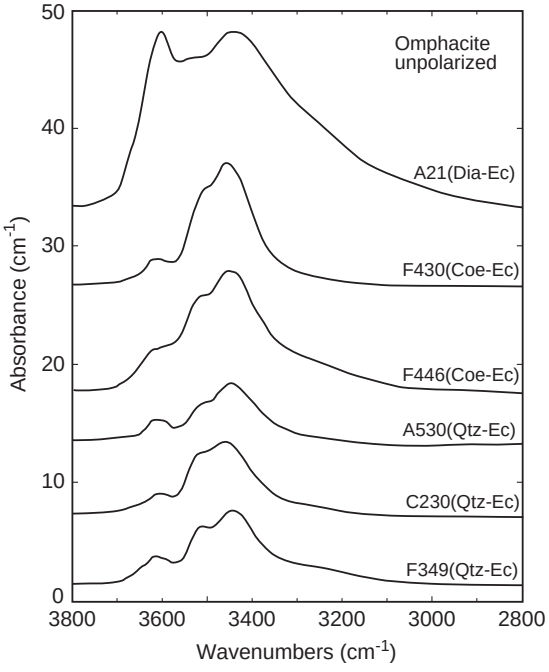

Fig. 3. Representative unpolarized infrared spectra of omphacite (modified after Katayama and Nakashima, 2003). Omphacite has three hydroxyl bands in the regions at 3440–3460, 3500–3530 and 3600–3625 cm^{-1}. The absorbance is normalized to 1 cm thickness.

4. Analytical methods for water content

Infrared spectra of these minerals were obtained between wavenumbers of 1000 and 4000 cm^{-1} using microscopic Fourier transform infrared (FTIR) spectrometers (JASCO MFT-2000 and IRT-30). Doubly polished sections were prepared with 100–40 μm thickness. The samples were measured with a Globar light source, KBr beam-splitter and an MCT detector. Several hundred scans were accumulated for each spectrum with 2 or 4 cm^{-1} resolution. We measured optically crack- and inclusions-free sample areas with apertures of 30×30 to 100×100 μm. A gold-wire grid polariser was applied to some oriented crystals.

SIMS analysis was performed using Cameca ims-3F. The samples were coated with a 20 nm thick layer of Au to eliminate electrostatic charging for the SIMS analysis. A primary ion beam consisting of mass-filtered ^{16}O, accelerated -14.5 keV to the samples with spot size of about 10 μm in diameter and a beam current of about 20 nA. The intensity of the positive secondary ^{1}H and ^{30}Si ions were measured under energy filtering by 200 cycles to obtain steady state secondary ion emissions. To reduce the background signals, the vacuum level of the sample chamber was maintained at 0.2 μPa, and a cold trap by liquid nitrogen was employed. For the quantitative analysis, we prepared standard minerals of augite (160 ppm H_2O by weight), pyrope (30 ppm H_2O) and hornblende (1.66 wt.% H_2O). These standard minerals were measured repeatedly in every analysis of the sample to construct the calibration line with each analysis. Other analytical and instrumental conditions were similar to the previous work by Yurimoto et al. (1989).

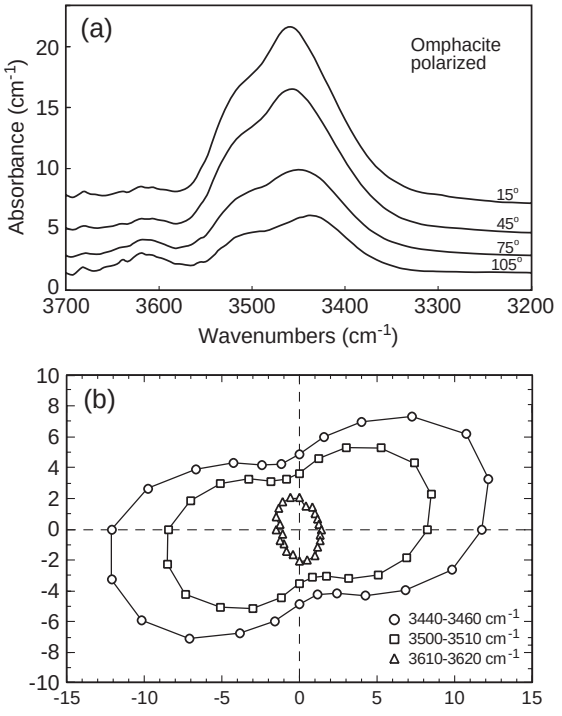

Fig. 4. (a) Polarized infrared spectra of an omphacite grain at different polarization orientation. (b) Absorption intensity distributions as a function of the polarization orientation of three hydroxyl bands. The axes are in arbitrary units.

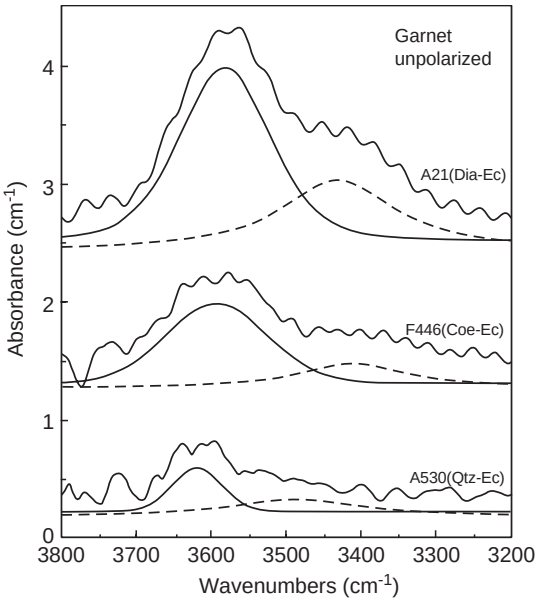

Fig. 5. Infrared spectra of garnet showing a band at 3600 cm^{-1} and a weak and broad band around 3400 cm^{-1}. The ~3400 cm^{-1} band is considered due to liquid-like molecular. Gaussian peak-fitting routine separates the spectra into two bands (solid and dotted lines). We used the 3600 cm^{-1} band area to calculate water content in garnet.

5. Results of water content analyses

5.1. Infrared spectra

IR unpolarized spectra of omphacite showed three hydroxyl absorption bands in the regions of 3440–3460, 3500–3530 and 3600–3625 cm^{-1} (Fig. 3). The 3440–3460 cm^{-1} band is typically the most intense,

and the 3600 cm^{-1} band the least intense in the spectrum. Similar hydroxyl band positions are reported in both synthetic and natural clinopyroxenes, with relative band intensities dependant on composition (Skogby et al., 1990; Smyth et al., 1991; Bromiley and Keppler, 2004; Bromiley et al., 2004a). For omphacitic pyroxene, the 3440–3460 cm^{-1} band is predominated in the spectrum with strong polarization of maximum absorption in the γ direction (Smyth et al., 1991). In our measurements, the relative absorbances of the hydroxyl bands are variable for different grains of the same samples. This is attributed to different orientations of different grains with respect to the infrared beam direction. We have attempted to overcome this variability by measuring large numbers of grains (~30) and averaging the results. This average also incorporates any real variability in absolute or relative absorbance of the hydroxyl bands. Infrared spectra of the diamond-grade omphacite are somewhat broader than those from the other samples. These omphacites show abundant quartz exsolutions and our IR analysis includes the inclusions. Thus the total absorbance may also reflect water from the exsolved quartz that formed by the breakdown of the Ca–Eskola component. Polarized spectra using a gold-wire grid polarizer showed significant differences in the hydroxyl absorbances with polarized orientations (Fig. 4). The maximum intensity of the 3450 and 3500 cm^{-1} bands has the same orientation; in contrast, the 3600 cm^{-1} band shows the highest intensity perpendicular to the other bands, indicating that the OH dipoles in omphacite have different orientations (Fig. 4). Koch-Müller et al. (2004) interpreted the 3600 cm^{-1} band in clinopyroxene to be related to nm-size inclusions based on TEM observations and synchrotron IR spectroscopy. This possibility cannot be ruled out in our analyses, particularly on the diamond-grade pyroxene that contains quartz exsolution. However, water solubility experiments on Jd–Di–CaEs pyroxene solutions showed that the hydroxyl-stretching band at 3600 cm^{-1} is due to hydrogen occupied in the M_2 site vacancy (Bromiley and Kep-

Table 3
Results of FTIR and SIMS analyses

Sample	Rock type	Minerals	FTIR analysis			SIMS analysis		
			Integral absorbance (cm^{-1})	H_2O content (ppm wt)*		$H/10^3Si$ atomic ratio	H_2O content (ppm wt)	Bulk-rock water (H_2O ppm wt)
A21	Dia–Ec	Omp	3720	1650 ± 500	Matrix	10.26 ± 3.57	870 ± 320	
					Inclusion	10.46 ± 0.45	890 ± 40	
		Grt	210 ± 45	150 ± 30	Matrix	2.13 ± 0.34	130 ± 20	
		Rt	n.d.	n.d.				460 ± 30
F430	Coe–Ec	Omp	2732	1210 ± 360	Matrix	5.34 ± 0.76	440 ± 60	
		Grt	155 ± 19	110 ± 20	Matrix	1.37 ± 0.1	80 ± 10	
		Rt	961	620				300 ± 20
F446	Coe–Ec	Omp	2143	950 ± 270	Matrix	4.91 ± 1.34	400 ± 110	
		Grt	169 ± 41	120 ± 30	Matrix	1.65 ± 0.28	100 ± 20	
		Rt	n.d.	n.d.				590 ± 30#
A530	Qtz–Ec	Omp	1264	560 ± 170	Matrix	3.50 ± 0.12	290 ± 10	
		Grt	75 ± 47	50 ± 30	Matrix	0.67 ± 0.48	40 ± 20	
		Rt	1153	740				3070 ± 30#
C230	Qtz–Ec	Omp	1010	450 ± 130	Matrix	2.84 ± 0.19	230 ± 20	
		Grt	89 ± 47	60 ± 30	Matrix	0.67 ± 0.48	50 ± 40	
		Rt	507	330				2600 ± 50#
F349	Qtz–Ec	Omp	1098	490 ± 150	Matrix	2.77 ± 0.24	230 ± 20	
		Grt	70 ± 46	50 ± 30	Matrix	0.18 ± 0.08	10 ± 5	
		Rt	n.d.	n.d.				1730 ± 20#
PO115	Whiteschist	Coe	n.d.	n.d.	Inclusion	3.8 ± 0.6	<10 ppm	
DB94	Coe–Ec	Coe	n.d.	n.d.	Inclusion	3.6	<10 ppm	

*Hydroxyl content in the FTIR analysis was calculated by using reported molar absorption coefficient (Bell et al., 1995). Error in omphacite was estimated as ~30% of average of 30 grains. Others are statistical error in analyses. # Water from hydrous minerals was added in the bulk total water content.

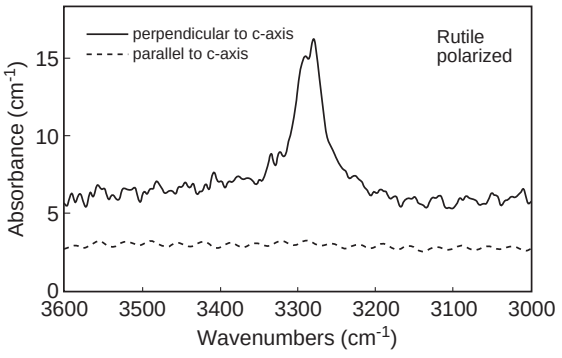

Fig. 6. Polarized infrared spectra of rutile from the coesite–eclogite show strong pleochroism. The absorption intensity at 3280 cm^{-1} is maximum when the polarized orientation is perpendicular to the tetragonal *c*-axis and minimum at parallel to the *c*-axis.

pler, 2004). Different orientations of the OH dipole are also reported in diopside (Ingrin et al., 1989; Skogby et al., 1990), and interpreted as several distinct hydrogen sites in the clinopyroxene structure.

Garnets show hydroxyl absorption at 3400–3700 cm^{-1}, which consists of an intense band at 3600 cm^{-1} and a weak broad band around 3400 cm^{-1} (Fig. 5). The 3600 cm^{-1} band is close to those found in mantle xenoliths (Aines and Rossman, 1984a; Bell and Rossman, 1992b), and considered to result from OH-vibrations of the tetrahedral site in garnet like those observed in hydrogrossular. The intensity of the 3400 cm^{-1} broad band is heterogeneous in garnet crystals and significantly increases when the inclusion-rich domains were analyzed. Therefore, this band is most likely due to liquid-like molecular water such as submicroscopic fluid inclusions. We attempted to model the spectra using a Gaussian peak-fitting routine to eliminate such water content (Fig. 5). We calculated intrinsic hydroxyl absorption in the garnets using the band at 3600 cm^{-1} (Table 3).

Rutiles are characterized by a sharp absorption band centered at 3280 cm^{-1} and show strong anisotropic behavior (Fig. 6). Maximum absorption occurs when the electric vector of the polarized radiation is perpendicular to the tetragonal *c*-axis, although the absorbance parallel to the *c*-axis is extremely small (practically zero) compared to the absorbance perpendicular to the *c*-axis. Similar observations are reported in other natural rutiles from several different geological environments (Rossman and Smyth, 1990; Hammer and Beran, 1991; Vlassopoulos et al., 1993). The hydroxyl absorbances in our rutiles vary among the different samples (Table 3), but the diamond-grade rutile does not show any detectable hydroxyl absorbance.

Coesites from Western Alps and Dabie–Sulu terranes show no detectable hydroxyl absorbance in their IR spectra. Rossman and Smyth (1990) also reported absence of hydrogen peaks in natural coesites from the kimberlite xenoliths, although synthesized coesite shows sharp hydroxyl bands at 3575, 3515, 3460 cm^{-1} and contains up to 200 ppm H_2O (Mosenfelder, 2000; Koch-Müller et al., 2001).

5.2. SIMS analysis

Surface-adsorbed water is important to eliminate prior to any trace hydrogen analysis of nominally anhydrous minerals. Depth profiling measurements by SIMS can easily remove the contribution of such water at the sample surface. Fig. 7 shows typical profiling of Si and H ions of omphacite and garnet.

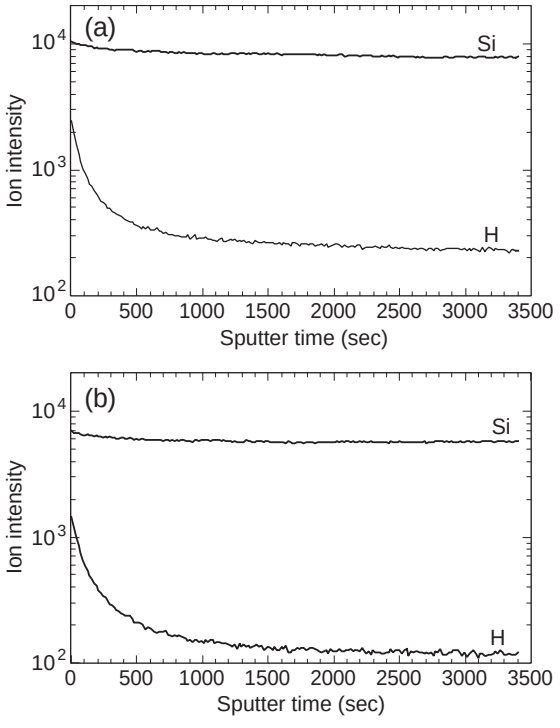

Fig. 7. Secondary ion intensities of H and Si of omphacite (a) and garnet (b) as a function of sputter time.

The hydrogen ion intensity rapidly decreases with sputter time and reaches steady state, which corresponds to the hydrogen concentration in crystals. The hydrogen intensities are normalized to those of Si to compensate measurement condition changes during and among analysis sessions. Using standard minerals, we constructed calibration lines for each analysis. Estimated water contents are listed in Table 3. Omphacites contain 230–870 ppm H_2O (by weight), and garnets contain 10–130 ppm H_2O. The SIMS results show good correlation with the hydroxyl absorbances analyzed by infrared analyses (Table 3). Coesites show lower hydrogen counts than the standard quartz, which contains 10 ppm H_2O. This agrees with the absence of hydroxyl absorbance in the IR analysis. Note that the SIMS spot analysis can measure water content in the micro-scale inclusions. We analyzed omphacite inclusions in zircon, which contain higher Ca–Eskola component, and found to contain similar water contents (~890 ppm H_2O) compared to the matrix omphacite from same sample.

6. Discussions

6.1. Quantitative calibration of hydroxyl content

Infrared spectroscopy is the most frequently used technique to determine trace hydroxyl components in nominally anhydrous minerals because of its high sensitivity in the frequencies of hydroxyl stretching vibrations and its ability to distinguish structurally incorporated OH in minerals. To calculate the water content from the IR spectrum, an independent method is needed to quantify the water concentration, such as P_2O_5 cell coulometry (Wilkins and Sabine, 1973), gravimetric techniques (Aines and Rossman, 1984b), nuclear reaction analysis (Rossman et al., 1988) or gas extraction manometry (Bell et al., 1995). After using one of these methods for calibration, one can estimate water concentration in minerals from an infrared spectrum according to Lambert–Beer's law as follows

$$C_{OH} = \frac{1}{\varepsilon\gamma d}\int K(\nu)\mathrm{d}\nu$$

where C_{OH} is the water concentration in analyzed minerals, expressed as moles per liter, $K(\nu)$ is the absorption intensity (absorbance) of the water as a function of wavenumber ν, ε is the molar absorption coefficient, γ is the orientation factor, which depends on crystallographic anisotropy, and d is the sample thickness. The molar absorption coefficient ε is determined for specific minerals using one of the independent calibration methods and an infrared spectrum.

To estimate the water concentration in the omphacite, we first used a reported molar absorption coefficient for clinopyroxene (augite) by Bell et al. (1995) and an orientation factor of 1/3 for the unpolarized IR spectra. The integral hydroxyl absorbance yields 1650 ppm H_2O by weight for the diamond-grade eclogite, 1210–950 ppm H_2O for the coesite–eclogites, and 560–490 ppm H_2O for the quartz–eclogites (Table 3). However, the direct application of the augite calibration to the omphacite is questionable, because the IR spectra between augite and omphacite are significantly different. Paterson (1982) reported that the molar absorption coefficient has frequency dependence for a variety of substantially hydrous materials and compounds. Libowizky and Rossman (1997) also reported a similar relation from stoichiometric hydrous silicate and oxide minerals. The higher frequency of the hydroxyl bands in omphacite compared to augite may result in a significant overestimate of the water content in omphacite. In this study, we determined the hydrogen concentration of the omphacites using SIMS, which yields 870 ppm H_2O (by weight) for the diamond-grade eclogite, 440–400 ppm H_2O for the coesite–eclogites, and 290–230 ppm H_2O for the quartz–eclogites (Table 3). These SIMS results show good correlation with the IR analysis (Fig. 8a), although the water content is approximately half of that calculated from the infrared spectra. The discrepancy is likely due to the IR calibration applied to the calculations as mentioned above. Using the water concentration determined by SIMS, we calculated a molar absorption coefficient for omphacite and obtained $8.34 \pm 1.46 \times 10^4$ (L/mol/cm^2). This value is approximately twice as large as the molar absorption coefficient of augite, but it is similar to that inferred from the frequency dependent calibration (Fig. 9).

The IR spectra of garnets yield 150 ppm H_2O for the diamond-grade eclogite, 120–110 ppm H_2O for the coesite–eclogites, and 60–50 ppm H_2O for the quartz–eclogites (Table 3), based on an integral

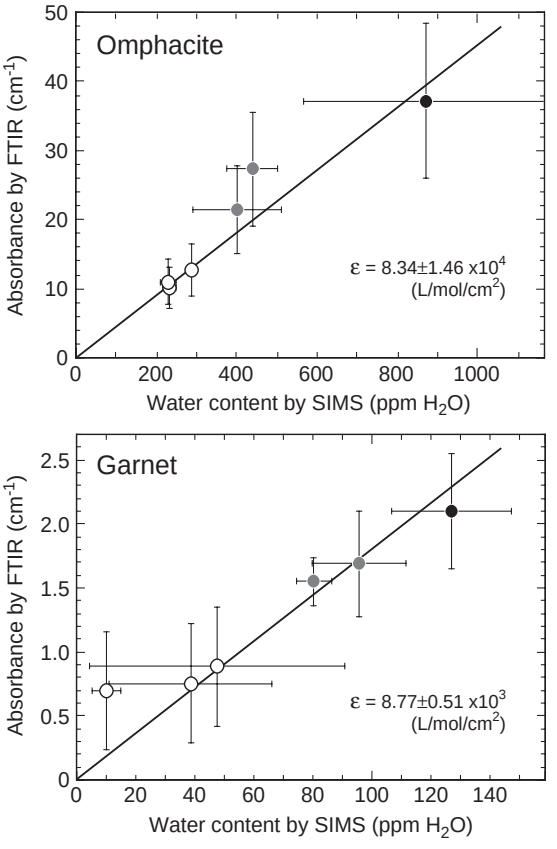

Fig. 8. IR integral absorbance versus water content measured by SIMS analysis for omphacite (a) and garnet (b). Both data sets show quasi-liner relations and resultant absorption coefficients are $8.34 \pm 1.46 \times 10^4$ (L/mol/cm^2) for omphacite and $8.77 \pm 0.51 \times 10^3$ (L/mol/cm^2) for garnet. Black symbol is the diamond-grade eclogite, gray is the coesite–eclogite and open symbol is the quartz eclogite.

molar absorption coefficient for pyrope (Bell et al., 1995). Most garnets in previous works show similar hydroxyl peaks and calibrations (Aines and Rossman, 1984a; Rossman and Aines, 1991; Bell et al., 1995). The SIMS analysis results in similar water contents (Fig. 8b). When we used the IR and SIMS results, a molar absorption coefficient of $8.77 \pm 0.51 \times 10^3$ (L/mol/cm^2) was obtained for garnet. The coefficient is similar to that reported in previous studies, although it is significantly lower than that of the frequency dependent calibration (Fig. 9). This indicates the importance of individual calibrations for quantitative analysis of trace amounts of water in the nominally anhydrous minerals.

6.2. Water content dependence with metamorphic conditions

The water contents in both omphacite and garnet systematically increase with increasing metamorphic pressure (Fig. 10). Omphacite contains abundant cation vacancies, which increases with pressure up to 9 mol% Ca–Eskola component. Thus the water concentration shows a correlation with the vacancy in the pyroxene structure. A similar relationship has also been reported in clinopyroxenes from the mantle-derived eclogite in the Roberts Victor kimberlite (Smyth et al., 1991). Bromiley and Keppler (2004) synthesized Na-rich clinopyroxenes under water-saturated conditions and found increasing water solubility with the M_2 site vacancy concentration. These results indicate that the M_2 site vacancy is the most dominant mechanism for hydrogen incorporation in omphacite. The Ca–Eskola component becomes unstable at low pressures, which results decrease the number of M_2 site vacancy and hence decrease water solubility in clinopyroxene. This may explain the occurrences of minute fluid inclusions that occur in the core of omphacite from UHP–HP eclogites (e.g., Scambelluri and Philippot, 2001).

Garnet shows a hydroxyl peak at ~3600 cm^{-1} (Fig. 5), which is commonly found in natural garnets, and it is considered to be a $(O_4H_4)^{4-}$ cluster at the tetrahe-

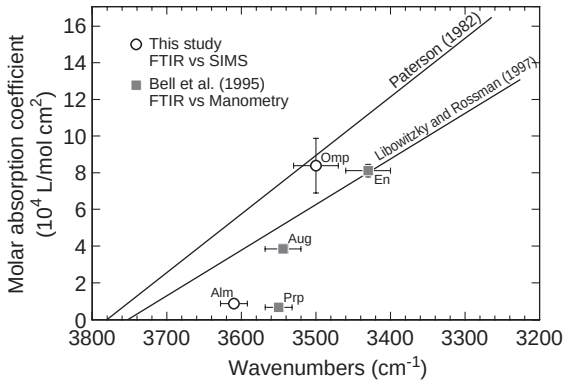

Fig. 9. Molar absorption coefficient for each mineral as a function of averaged wavenumber of hydroxyl stretching bands. The frequency dependent calibrations by Paterson (1982) and Libowizky and Rossman (1997) are shown. The molar absorption coefficients of omphacite (Omp) and almandin-rich garnet (Alm) were calculated from the results of FTIR and SIMS analyses in this study. The coefficients of enstatite (En), augite (Aug) and pyrope (Prp) from Bell et al. (1995) are also shown for comparison.

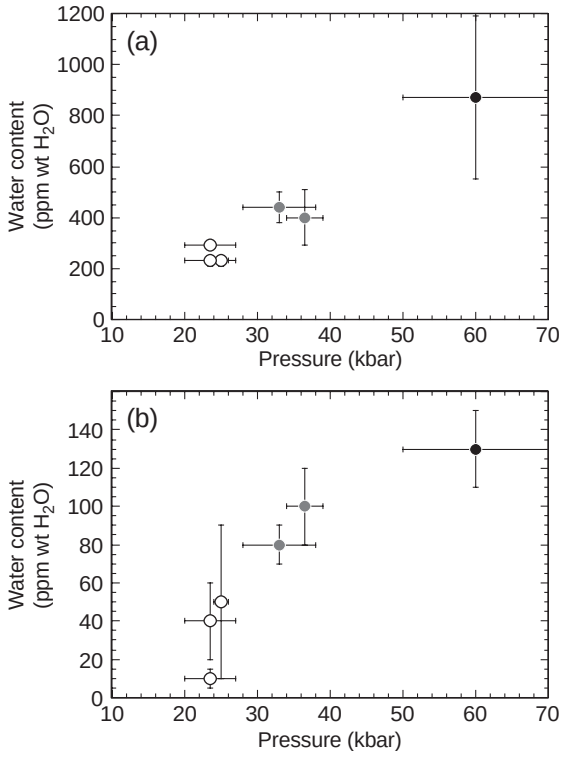

Fig. 10. Pressure dependence of water contents (ppm wt H_2O) in omphacite (a) and garnet (b) of each eclogite. The water content in both omphacite and garnet increases with pressure of the host eclogite.

dral site. The centered wavenumber of the hydroxyl peak in garnet slightly changes with pressure; the 3580 cm^{-1} peak in the diamond–eclogite shifts to 3620 cm^{-1} in the quartz–eclogite. The hydroxyl stretching frequency is correlated to the hydrogen bonding distance (Nakamoto et al., 1955; Libowitzky, 1999). A stronger field of hydrogen bonding in grossular-rich garnet due to substitution of Mg^{2+} into the dodecahedral position by larger Ca^{2+} may explain the peak shift in garnet. Although our results clearly show that the water content in garnet increases with increasing metamorphic grade, experimental studies on water solubility in garnet are controversial. Lu and Keppler (1997) reported that water solubility in pyrope increases with pressure up to 10 GPa. In contrast, Withers et al. (1998) showed no detectable hydrogen in pyrope above 7 GPa.

Water contents in rutile were calculated from polarized spectra along different crystal axis using an anisotropic relation of the absorbance; $A_{total} = 2A_{perpendicular\ to\ c} + A_{parallel\ to\ c}$. Using a molar absorption coefficient reported by Hammer and Beran (1991), the rutile contains up to 740 ppm H_2O (Table 3). The water content in the rutile is variable in the different samples, but it is important to note that the diamond-grade rutile shows no hydroxyl absorption. Bromiley et al. (2004b) reported no detectable hydrogen in synthesized α-PbO_2 type TiO_2 in contrast to variable water content in the rutile structure. The absence of hydroxyl bands in the diamond-grade rutile may indicate that formed a high-pressure polymorph with a α-PbO_2 type structure. This type of TiO_2 phase has been reported in ultrahigh-pressure metamorphic rocks from the Saxonian Erzgebirge, Germany (Hwang et al., 2000). Laser Raman spectra of the TiO_2 phase show a rutile structure, however, the original structural evidence may be obliterated during exhumation because the α-PbO_2 structure is highly unstable at ambient conditions (Hwang et al., 2000).

According to the results of our water content analyses, we calculated a partition coefficient for water between garnet and omphacite. The partition coefficient is more or less constant $D^{Grt/Omp}$~0.2–0.1, with a slight decrease at high pressure (Fig. 11). This means that water prefers to dissolve into omphacite rather than garnet in deeply subducted oceanic crust. Although the volume of the omphacite decreases in the eclogite with increasing pressure, as it dissolves into majoritic garnet at high pressures (Irifune et al., 1986), the total water con-

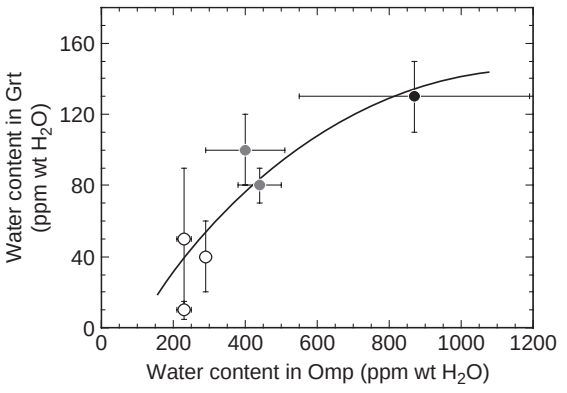

Fig. 11. Partitioning coefficient of water content between omphacite and garnet in each eclogite. The partitioning of water content is similar in the different eclogites ($D^{Grt/Omp}$~0.1–0.2), but decreases slightly at high pressure.

tent in the eclogite remains stable due to increasing water solubility in the garnet (Table 3).

Hydrogen is a very mobile element, whose diffusion rate is several orders of magnitudes faster than that of major elements (e.g., Wang et al., 1996; Carpenter et al., 2000). Thus the water in crystals may be easily lost or added. It is therefore difficult to eliminate the possibility of later-stage water incorporation during the retrograde metamorphism related to exhumation. However, we analyzed the water contents of the zircon-hosted inclusions, which are less affected by later events. They contain similar amounts of water compared to that of the matrix minerals (Table 3). Recently, Bell and Ihinger (2000) measured the isotopic composition of hydrogen in nominally anhydrous minerals. Such analysis could be a key for further discussion on the origin of the trace amounts of water in these minerals.

6.3. Water content in the deep subducted oceanic crust

Here we report water contents for the subducted oceanic crust, using natural samples that experienced subduction zone metamorphism at depths up to ~180 km. At relatively shallow depths (25–35 km), basaltic crust is mostly composed of hydrous minerals, such as amphibole and epidote group minerals. The subducting crust therefore contains significant amounts of water (1.6~2.0 wt.% H_2O) at these depths (Fig. 12). Most of the water in oceanic crust would be released at less than ~50 km depth due to the breakdown of amphibole (e.g., Poli, 1993). However, even after such dehydration reactions occur in the basaltic crust, trace amounts of water can still survive within nominally anhydrous minerals, such as omphacite, garnet and rutile. Considering the modal proportions of eclogite, 460 ppm wt H_2O is shown to exist in the diamond-grade eclogite, although no hydrous minerals are stable (Table 3). The eclogites transform to garnetite around 400 km depth, which is mainly composed of majoritic garnet and stishovite (e.g., Irifune et al., 1986). Water solubility experiments show that these high-pressure phases can dissolve trace amounts of water, up to ~700 ppm H_2O in majorite (Katayama et al., 2003) and ~800 ppm H_2O in stishovite (Chung and Kagi, 2002; Panero et al., 2003). Consequently, the water in the eclogites can be transferred to the majorite and stishovite, and thus can be carried into

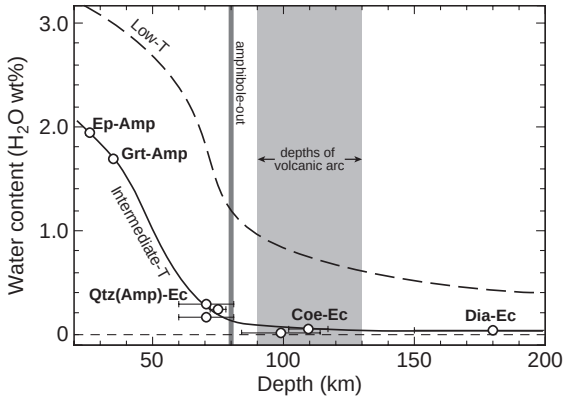

Fig. 12. Depth profile of water content in the subducting basaltic crust. Open circle represents water content of natural samples from the Kokchetav UHP–HP massif, which *P–T* conditions are similar to the intermediate geotherm. Water content along the low-temperature geotherm is based on experimental results by Schmidt and Poli (1998). The depths of volcanic front have been reported to be constant at around 110 km in most subduction zones (Tatsumi, 1986), whereas most dehydration in the subducted oceanic crusts occurs beneath the fore-arc region. Even deeper than the depths of volcanic arcs, trace amounts of water are transported by nominally anhydrous minerals beyond the stability of hydrous minerals.

the mantle transition zone. The amount of water carried by descending oceanic crust into the deep mantle is relatively small (~460 ppm H_2O), but it is known that even a trace amount of water play an important role in the geodynamics in the Earth's interior, via its effects on the melting behavior and physical properties of minerals. For example, several tens of ppm H_2O in the mantle can modify plasticity and electrical conductivity by a few orders of magnitude (e.g., Karato, 1990; Hirth and Kohlstedt, 1996) and change the lattice-preferred orientation of olivine and the resultant seismic anisotropy in the upper mantle (Jung and Karato, 2001). At the mantle transition zone, wadsleyite and ringwoodite can dissolve considerable amounts of water (Inoue et al., 1995; Kohlstedt et al., 1996). Water transported by majoritic garnet in subducted oceanic crust may spread into the surrounding mantle peridotites at these depths. Some seismological evidences suggest that several hundreds of ppm H_2O might exist in the mantle transition zone (e.g., Wood, 1995). In addition, petrological and geochemical studies on erupted volcanic rocks in mid-oceanic ridge and hotspots found that the source regions likely contain significant amounts of water (Garcia et al., 1989; Sobolev and Chaussidon, 1996; Hauri, 2002).

The present study demonstrated that considerable amounts of water are incorporated in nominally anhydrous minerals such as omphacite, garnet and rutile in eclogite beyond the stability of hydrous minerals. Such water in subducted oceanic crust may be further transported into the deep regions of a subduction zone, and may provide a repository for volatiles in the mantle and consequently play an important role in the mantle dynamics of the Earth's interior.

Acknowledgements

We thank S. Maruyama, K. Hirose and S. Karato for many discussions. Constructive comments on the early version by H. Keppler, A. Berry and P. Skemer helped to improve the manuscript. This paper benefited from journal reviews by two anonymous reviewers. This study was supported by the Japan Society for the Promotion of Science.

References

Ackermann, L., Cemic, L., Langer, K., 1983. Hydrogarnet substitution in pyrope: a possible location for water in the mantle. Earth Planet. Sci. Lett. 62, 208–214.

Aines, R.D., Rossman, G.R., 1984a. Water content of mantle garnets. Geology 12, 720–723.

Aines, R.D., Rossman, G.R., 1984b. The hydrous component in garnets: pyralspites. Am. Mineral. 69, 1116–1126.

Bell, D.R., Rossman, G.R., 1992a. Water in Earth's mantle: the role of nominally anhydrous minerals. Science 255, 1391–1397.

Bell, D.R., Rossman, G.R., 1992b. The distribution of hydroxyl in garnets from the subcontinental mantle of southern Africa. Contrib. Mineral. Petrol. 111, 161–178.

Bell, D.R., Ihinger, P.D., 2000. The isotopic composition of hydrogen in nominally anhydrous mantle minerals. Geochim. Cosmochim. Acta 64, 2109–2118.

Bell, D.R., Ihinger, P.D., Rossman, G.R., 1995. Quantitative analysis of trace OH in garnet and pyroxenes. Am. Mineral. 80, 465–474.

Bohlen, S.R., Boettcher, A.L., 1982. The quartz–coesite transformation: a pressure determination and effects of other components. J. Geophys. Res. 87, 7073–7078.

Bromiley, G.D., Keppler, H., 2004. An experimental investigation of hydroxyl solubility in jadeite and Na-rich clinopyroxenes. Contrib. Mineral. Petrol. 147, 189–200.

Bromilet, G.D., Keppler, H., McCammon, C., Bromiley, F., Jacobse, S., 2004a. Hydrogen solubility and speciation in natural, gem-quality chromian diopside. Am. Mineral. 89, 941–949.

Bromiley, G.D., Hilaret, N., McCammon, C., 2004b. The solubility of hydrogen and ferric iron in rutile and TiO_2 (II): implications for phase assemblages during ultrahigh-pressure metamorphism and for the stability of silica polymorphs in the lower mantle. Geophys. Res. Lett. 31, doi:10.1029/2004GL019430.

Bundy, F.P., 1980. The *P*, *T* phase and reaction diagram for elemental carbon. J. Geophys. Res. 85, 6930–6936.

Carpenter, S.J., Mackwell, S.J., Dyar, M.D., 2000. Hydrogen in diopside diffusion profiles. Am. Mineral. 85, 480–488.

Carswell, D.A., O'Brien, P.J., Wilson, R.N., Zhai, M., 1997. Thermobarometry of phengite-bearing eclogites in the Dabie Mountains of central China. J. Metamorph. Geol. 15, 239–252.

Chung, J., Kagi, H., 2002. High concentration of water in stishovite in the MORB system. Geophys. Res. Lett. 29, doi:10.1029/2002GL015579.

Dobretsov, N.L., Sobolev, N.V., Shatsky, V.S., Coleman, R.G., Ernst, W.G., 1995. Geotectonic evolution of diamondiferous paragneisses, Kokchetav Complex, northern Kazakhstan: the geologic enigma of ultrahigh-pressure crustal rocks within a Paleozoic foldbelt. Isl. Arc 4, 267–279.

Ellis, D.J., Green, D.H., 1979. An experimental study of the effect of Ca upon garnet–clinopyroxene Fe–Mg exchange equilibria. Contrib. Mineral. Petrol. 71, 13–22.

Garcia, M.O., Muenow, D.W., Aggrey, K.E., O'Neil, J.R., 1989. Major element, volatile, and stable isotope geochemistry of Hawaiian submarine tholeiitic glasses. J. Geophys. Res. 94, 10525–10538.

Geiger, C.A., Langer, K., Bell, D.R., Rossman, G.R., Winkler, B., 1991. The hydroxide component in synthetic pyrope. Am. Mineral. 76, 49–59.

Hammer, V.M.F., Beran, B., 1991. Variations in the OH concentration of rutiles from different geological environments. Mineral. Petrol. 45, 1–9.

Hauri, E., 2002. SIMS analysis of volatiles in silicate, 2: isotopes and abundances in Hawaiian melt inclusions. Chem. Geol. 183, 115–141.

Hirth, G., Kohlstedt, D.L., 1996. Water in the oceanic upper mantle: implications for rheology, melt extraction and the evolution of the lithosphere. Earth Planet. Sci. Lett. 144, 93–108.

Holland, T.J.B., 1980. The reaction albite=jadeite+quartz determined experimentally in the range 600–200 °C. Am. Mineral. 65, 129–134.

Hwang, S.L., Shen, P., Chu, H.T., Yui, T.Y., 2000. Nanometer-size α-PbO_2-type TiO_2 in garnet: a thermobarometer for ultrahigh-pressure metamorphism. Science 288, 321–324.

Ingrin, J., Latrous, K., Doukhan, J.C., Doukhan, N., 1989. Water in diopside: electron microscopy and infrared spectroscopy study. Eur. J. Mineral. 1, 327–341.

Inoue, T., Yurimoto, H., Kudoh, Y., 1995. Hydrous modified spinel, $Mg_{1.75}SiH_{0.5}O_4$: a new water reservoir in the mantle transition region. Geophys. Res. Lett. 22, 117–120.

Irifune, T., Sekine, T., Ringwood, A.E., Hibberson, W.O., 1986. The eclogite–garnetite transformation at high pressure and some geophysical implications. Earth Planet. Sci. Lett. 77, 245–256.

Iwamori, H., 1998. Transportation of H_2O and melting in subduction zones. Earth Planet. Sci. Lett. 160, 65–80.

Jung, H., Karato, S., 2001. Water-induced fabric transitions in olivine. Science 293, 1460–1463.

Kaneko, Y., Maruyama, S., Terabayashi, M., Yamamoto, H., Ishikawa, M., Anma, R., Parkinson, C.D., Ota, T., Nakajima, Y., Katayama, I., Yamamoto, J., Yamauchi, K., 2000. Geology of the Kokchetav UHP–HP metamorphic belt, northern Kazakhstan. Isl. Arc 9, 264–283.

Karato, S., 1990. The role of hydrogen in the electrical conductivity of the upper mantle. Nature 347, 272–273.

Karato, S., 2003. Mapping water content in the upper mantle. In: Eiler, J. (Ed.), Inside the Subduction Factory. American Geophysical Union, pp. 135–152.

Katayama, I., Nakashima, S., 2003. Hydroxyl in clinopyroxene from the deep subducted crust: evidence for H_2O transport into the mantle. Am. Mineral. 88, 229–234.

Katayama, I., Zayachkovsky, A.A., Maruyama, S., 2000a. Progressive *P–T* records from zircon in Kokchetav UHP–HP rocks, northern Kazakhstan. Isl. Arc 9, 417–428.

Katayama, I., Parkinson, C.D., Okamoto, K., Nakajima, Y., Maruyama, S., 2000b. Supersilicic clinopyroxene and silica exsolution in UHPM eclogite and pelitic gneiss from the Kokchetav massif, Kazakhstan. Am. Mineral. 85, 1368–1374.

Katayama, I., Maruyama, S., Parkinson, C.D., Terada, K., Sano, Y., 2001. Ion micro-probe U–Pb zircon geochronology of peak and retrograde stages of ultrahigh-pressure metamorphic rocks from the Kokchetav massif, northern Kazakhstan. Earth Planet. Sci. Lett. 188, 185–198.

Katayama, I., Hirose, K., Yurimoto, H., Nakashima, S., 2003. Water solubility in majoritic garnet in subducting oceanic crust. Geophys. Res. Lett. 30, doi:10.1029/2003GL018127.

Koch-Müller, M., Fei, Y., Hauri, E., Liu, Z., 2001. Location and quantitative analysis of OH in coesite. Phys. Chem. Miner. 28, 693–705.

Koch-Müller, M., Matsyuk, S., Wirth, R., 2004. Hydroxyl in omphacitic clinopyroxenes of upper mantle to lower crustal origin beneath the Siberian platform. Am. Mineral. 89, 921–931.

Kohlstedt, D.L., Keppler, H., Rubie, D.C., 1996. Solubility of water in the α, β and γ phases of $(Mg,Fe)_2SiO_4$. Contrib. Mineral. Petrol. 123, 345–357.

Libowitzky, E., 1999. Correlation of O–H stretching frequencies and O–H...O hydrogen bond lengths in minerals. Monatsh. Chem. 130, 1047–1059.

Libowizky, E., Rossman, G.R., 1997. An IR absorbance calibration for water in minerals. Am. Mineral. 82, 1111–1115.

Lu, R., Keppler, H., 1997. Water solubility in pyrope to 100 kbar. Contrib. Mineral. Petrol. 129, 35–42.

Maruyama, S., Liou, J.G., Terabayashi, M., 1996. Blueschists and eclogites of the world and their exhumation. Int. Geol. Rev. 38, 485–594.

Mosenfelder, J.L., 2000. Pressure dependence of hydroxyl solubility in coesite. Phys. Chem. Miner. 27, 610–617.

Nakamoto, K., Margoshes, M., Rundle, R.E., 1955. Stretching frequencies as a function of distances in hydrogen bonds. J. Am. Chem. Soc. 77, 6480–6486.

Ogasawara, Y., Ohta, M., Fukasawa, K., Katayama, I., Maruyama, S., 2000. Diamond-bearing and diamond-free metacarbonate rocks from Kumdy-Kol in the Kokchetav Massif, northern Kazakhstan. Isl. Arc 9, 400–416.

Okamoto, K., Maruyama, S., 1999. The high-pressure synthesis of lawsonite in the MORB+H_2O system. Am. Mineral. 84, 362–373.

Okamoto, K., Liou, J.G., Ogasawara, Y., 2000. Petrological study of the diamond grade eclogite in the Kokchetav massif, northern Kazakhstan. Isl. Arc 9, 379–399.

Omori, S., Liou, J.G., Zhang, R.Y., Ogasawara, Y., 1998. Petrogenesis of impure dolomitic marble from the Dabie Mountains, central China. Isl. Arc 7, 98–114.

Ono, S., 1998. Stability limits of hydrous minerals in sediment and mid-ocean ridge basalt compositions: implications for water transport in subduction zones. J. Geophys. Res. 103, 18253–18267.

Panero, W.R., Bemedetti, L.R., Jeanloz, R., 2003. Transport of water into the lower mantle: role of stishovite. J. Geophys. Res. 108, doi:10.1029/2002JB002053.

Paterson, M.S., 1982. The determination of hydroxyl by infrared absorption in quartz, silicate glasses and similar materials. Bull. Mineral. 105, 20–29.

Poli, S., 1993. The amphibolite–eclogite transformation — an experimental study on basalt. Am. J. Sci. 293, 1061–1107.

Poli, S., Schmidt, M.W., 1995. H_2O transport and release in subduction zones: experimental constraints on basaltic and andesitic systems. J. Geophys. Res. 100, 22299–22314.

Rauch, M., Keppler, H., 2002. Water solubility in orthopyroxene. Contrib. Mineral. Petrol. 143, 525–536.

Rossman, G.R., Aines, R.D., 1991. The hydrous components in garnets: grossular–hydrogrossular. Am. Mineral. 76, 1153–1164.

Rossman, G.R., Smyth, J.R., 1990. Hydroxyl contents of accessory minerals in mantle eclogites and related rocks. Am. Mineral. 75, 775–780.

Rossman, G.R., Rauch, F., Livi, R., Tombrello, T.A., Shi, C.R., Zhou, Z.Y., 1988. Nuclear reaction analysis of hydrogen in almandine, pyrope, and spessartine garnets. N. Jb. Mineral. Mh. H4, 172–178.

Scambelluri, M., Philippot, P., 2001. Deep fluids in subduction zones. Lithos 55, 213–227.

Schertl, H.P., Schreyer, W., Chopin, C., 1991. The pyrope–coesite rocks and their country rocks at Parigi, Dora Maira massif, western Alps: detailed petrography, mineral chemistry and *PT*-path. Contrib. Mineral. Petrol. 108, 1–21.

Schmidt, M.W., Poli, S., 1998. Experimentally based water budgets for dehydrating slabs and consequences for arc magma generation. Earth Planet. Sci. Lett. 163, 361–379.

Skogby, H., 1994. OH incorporation in synthetic clinopyroxene. Am. Mineral. 79, 240–249.

Skogby, H., Bell, D.R., Rossman, G.R., 1990. Hydroxide in pyroxene: variation in the natural environment. Am. Mineral. 75, 764–774.

Smyth, J.R., Bell, D.R., Rossman, G.R., 1991. Incorporation of hydroxyl in upper-mantle clinopyroxenes. Nature 351, 732–735.

Sobolev, A.V., Chaussidon, M., 1996. H_2O concentrations in primary melts from supra-subduction zones and mid-ocean ridges:

implications for H_2O storage and recycling in the mantle. Earth Planet. Sci. Lett. 137, 45–55.
Sobolev, N.V., Shatsky, V.S., 1990. Diamond inclusions in garnets from metamorphic rocks. Nature 343, 742–746.
Staudigel, H., Davies, G.R., Hart, S.R., Marchant, K.M., Smith, B.M., 1995. Large scale isotopic Sr, Nd and O isotopic anatomy of altered oceanic crust: DSDP/ODP sites 417/418. Earth Planet. Sci. Lett. 130, 105–120.
Tatsumi, Y., 1986. Formation of the volcanic front in the subduction zones. Geophys. Res. Lett. 17, 717–720.
Thompson, A.B., 1992. Water in the Earth's upper mantle. Nature 358, 295–302.
Vlassopoulos, D., Rossman, G.R., Haggerty, S.E., 1993. Coupled substitution of H and minor elements in rutile and the implications of high OH contents in Nb- and Cr-rich rutile from the upper mantle. Am. Mineral. 78, 1181–1191.
Wang, L., Zhang, Y., Essene, E., 1996. Diffusion of the hydrous component in pyrope. Am. Mineral. 81, 706–718.
Wilkins, R.W., Sabine, W., 1973. Water content of some nominally anhydrous silicates. Am. Mineral. 58, 508–516.
Withers, A.C., Wood, B.J., Carroll, M.R., 1998. The OH content of pyrope at high pressure. Chem. Geol. 147, 161–171.
Wood, B.J., 1995. The effect of H_2O on the 410-kilometer seismic discontinuity. Science 268, 74–76.
Yurimoto, H., Kurosawa, M., Sueno, S., 1989. Hydrogen analysis in quartz crystals and quartz glasses by secondary ion mass spectroscopy. Geochim. Cosmochim. Acta 53, 751–755.
Zhang, R.Y., Liou, J.G., Coleman, R.G., Ernst, W.G., Sobolev, N.V., Shatsky, V.S., 1997. Metamorphic evolution of diamond-bearing and associated rocks from the Kokchetav massif, northern Kazakhstan. J. Metamorph. Geol. 15, 479–496.